Automatic Control of Aircraft in Longitudinal Plane During Landing

Automatic control of aircraft during landing is discussed and a new structure of automatic landing system (ALS) is designed using the dynamic inversion concept and proportional-integral-derivative (PID) controllers in conventional and fuzzy variants. Theoretical results are validated by numerical simulations in the absence or presence of wind shears and sensor errors.

I. INTRODUCTION

The first automatic landing system (ALS) was designed in England in 1965. Most aircraft have ALSs based on the instrumental landing system (ILS) [1], using different conventional control laws: PD (proportional-derivative), PID (proportional-integral-derivative), or PI (proportional-integral) for the altitude and descent velocity control [2, 3], PD or PID laws for the pitch angle and pitch rate control, as well as different laws based on state vector, dynamic inversion concept, command filters, dynamic compensators, and state observers [4–7]. GPS use and the increase of the sensors' performances for the angular rates' measurement lead to the increase of the landing trajectory track accuracy [8, 9]. If a conventional control methodology is used, a linearized model of the nonlinear system should be previously developed; as a consequence, to obtain satisfactory control of a complex nonlinear system, nonlinear controllers should be developed [10].

This paper focuses on the automatic control of aircraft in the longitudinal plane, during landing, by using the linearized longitudinal dynamics of aircraft, considering the longitudinal and vertical wind shears [4] and the errors of the sensors. Our aim is to design a new ALS by using the dynamic inversion concept, command filters, and the altitude control after the state vector. In the design of the new landing system, the dynamic inversion method is chosen for its applicability to nonlinearities in the system and for its simplicity; on the other hand, the controllers of the same ALS have also been designed using the fuzzy logic because the controllers tuning can be made much finer by means of universe of discourse, number of membership functions, and their shapes, or chosen rules base.

Manuscript received June 24, 2012; revised October 11 and 18, 2012; released for publication November 2, 2012.

IEEE Log No. T-AES/49/2/944540.

Refereeing of this contribution was handled by M. Idan.

This work was supported by CNCSIS-UEFISCSU, Project PN II-RU, 1/28.07.2010, code TE_102/2010.

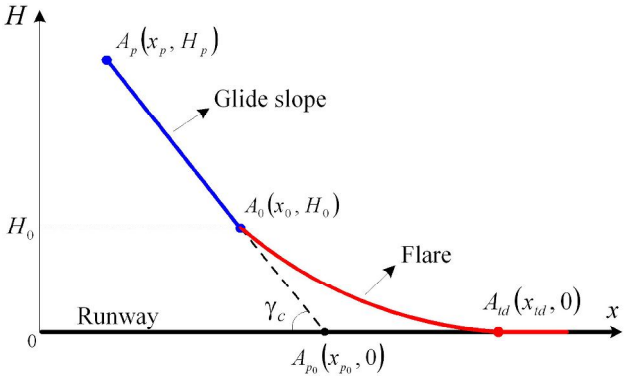

Fig. 1. Motion geometry during landing.

The contributions of this paper are: the general design of the new ALS structure including the longitudinal velocity control, the PID conventional controllers tuning for the altitude, pitch and velocity channels, the design of the above controllers in an intelligent approach by using the fuzzy techniques, the study of the errors induced by the wind shears and errors of the gyro sensors on both variants of the ALS (conventional and fuzzy). Theoretical results are validated by numerical simulations in the absence or presence of wind shears and sensor errors.

II. GEOMETRY OF THE LANDING IN LONGITUDINAL PLANE

The motion trajectory of aircraft in longitudinal plane, during landing, consists of the slope segment $\overline{A_pA_0}$ (Fig. 1).

The coordinate x_{p_0} is calculated by using the formula:

$$x_{p_0} = x_p - H_p/\tan(\gamma_c), \qquad \gamma_c < 0 \tag{1}$$

while the calculated altitude is obtained as follows:

$$H_c = \begin{cases} (x - x_{p_0})\cdot\tan(\gamma_c) & \text{for } H \geq H_0 = H_c(t_0) \\ H_0\cdot\exp((t_0 - t)/\tau) & \text{for } H < H_0 = H_c(t_0) \end{cases} \tag{2}$$

where τ is the time constant that defines the exponential curvature (flare landing phase), while t_0 is the time moment when the glide slope phase ends and the second landing phase begins. From the definition of the horizontal aircraft forward velocity $\dot{x}$ in the point with the coordinate x (flare curve), at a random time moment t ($t > t_0$), we get $t - t_0 = (x - x_0)/\dot{x}$, and, using this relationship, the second equation (2) gets the form:

$$H_c = H_0\exp((x_0 - x)/\tau\dot{x}), \qquad H < H_0: \tag{3}$$

Thus, the geometry of aircraft motion in the longitudinal plane, during landing, is described by the first equation (2), with x_{p_0} having the form (1)—glide slope phase, or by (3)—flare landing phase, with $\dot{x}$ having the form (= ® + °):

$$\dot{x} = V_x \cos\theta + V_z \sin = V_x \cos\theta + V_0 \sin® \sin \quad (4)$$

V_x and V_z are the aircraft velocity components along aircraft longitudinal axis (Ox) and normal axis (Ox), θ—pitch angle, ®—attack angle, and °—slope angle of aircraft trajectory.

The descent velocity H and the calculated one H_c (velocity that must be reached by the aircraft) are: $H = V_0 \sin°$, $H_c = V_0 \sin°_c \cong V_{x_c} \sin°_c$; V_0 is aircraft nominal velocity, V_{x_c}—calculated longitudinal velocity; during flare, we write: $\dot{H}_c = ¡ H_c/¿$, $\dot{H}_{c_0} = ¡ H_0/¿$. If V_0 and the coordinates of points A_p and A_0 are known, we calculate ¿, x_{p_0}, and x_{td}. If flare phase takes 5¿ s [1] and aircraft velocity is approximately constant during this landing phase, we obtain $x_{td} ¡ x_0 = V_0 ¢ 5¿$. Using the above equations and assuming $H_c = H_0$, we get $H_0 \cong ¡ V_0 ¿ \sin°_c$; $°_c$ is expressed in radians. According to Fig. 1, $H_0 = ¡ (x_{p_0} ¡ x_0) ¢ \tan°_c$. Also,

$$V_0 ¿ = (x_{p_0} ¡ x_0)/\cos°_c: \quad (5)$$

With the known values of x_0 and V_0, by means of (5) and $x_{td} ¡ x_0 = V_0 ¢ 5¿$, ¿ and x_{td} are obtained. In [2] ¿ is calculated with respect to the velocity $V_G = V_0 \cos° + V_{vx}$; V_{vx} is the wind velocity along longitudinal axis, depending on the descent rates $H_0 = H(x_0)$, $H_{td} = H(x_{td})$.

III. AIRCRAFT DYNAMICS IN LONGITUDINAL PLANE AND THE MODEL OF THE WIND SHEARS

The linear model of aircraft motion, in longitudinal plane, is described by the state equation $\dot{\mathbf{x}} = \mathbf{Ax} + \mathbf{Bu} + \mathbf{B_v v_v}$, with **x**—state vector (4 £ 1), **u**—command vector (2 £ 1), $\mathbf{v_v}$—vector of disturbances V_{vx} and V_{vz} (components of the wind velocity along the axes Ox and Oz [3, 4]), $\mathbf{x} = [V_x \; ® \; !_y \; \theta]^T$, $\mathbf{u} = [±_p \; ±_T]^T$, $\mathbf{v_v} = [V_{vx} \; V_{vz}]^T$. In the previous equations $!_y$ is the pitch angular rate, $±_p$—elevator deflection, $±_T$—engine command, while matrices **A**, **B**, $\mathbf{B_v}$ have the forms [5]:

$$\mathbf{A} = \begin{bmatrix} a_{11} & a_{12} & a_{13} & a_{14} \\ a_{21} & a_{22} & a_{23} & a_{24} \\ a_{31} & a_{32} & a_{33} & a_{34} \\ 0 & 0 & 1 & 0 \end{bmatrix} = \begin{bmatrix} X_u & X_w & 0 & ¡ g \cos_0 \\ Z_u^{\cdot} & Z_w & 1 & ¡ (g/V_0) \sin\theta_0 \\ \tilde{N}_u & \tilde{N}_w & \tilde{N}_q & \tilde{N}_\theta \\ 0 & 0 & 1 & 0 \end{bmatrix}$$

$$\mathbf{B} = \begin{bmatrix} b_{11} & b_{21} & b_{31} & 0 \\ b_{12} & b_{22} & b_{32} & 0 \end{bmatrix}^T = \begin{bmatrix} 0 & Z_{±_p}/V_0 & \tilde{N}_{±_p} & 0 \\ X_{±_T} & Z_{±_T}/V_0 & N_{±_T} & 0 \end{bmatrix}^T$$

$$\mathbf{B_v} = \begin{bmatrix} ¡ a_{11} & ¡ a_{21} & ¡ a_{31} & 0 \\ ¡ a_{12}^{\cdot} & ¡ a_{22}^{\cdot} & ¡ a_{32}^{\cdot} & 0 \end{bmatrix}^T = \begin{bmatrix} ¡ a_{11} & ¡ a_{21} & ¡ a_{31} & 0 \\ ¡ a_{12}/(57.3V_0) & ¡ a_{22}/(57.3V_0) & ¡ a_{32}/(57.3V_0) & 0 \end{bmatrix}^T.$$

Elements of the matrices **A**, **B**, $\mathbf{B_v}$ have been calculated using the equations in [5], with respect to the chosen aircraft stability derivates. Wind shears' modeling is presented in [4]:

$$V_{vx} = ¡ V_{vx_0} \sin(!_0 t), \qquad V_{vz} = ¡ V_{vz_0} [1 ¡ \cos(!_0 t)],$$
$$!_0 = 2¼/T_0 \quad (6)$$

where T_0 is the flight time inside the wind shear; the aircraft faces head wind and rear wind combined with vertical wind.

IV. AUTOMATIC CONTROL OF AIRCRAFT IN LONGITUDINAL PLANE USING DYNAMIC INVERSION

For the new ALS design, because a quantitative nonlinear description of the longitudinal dynamics was not available, we used the linearized dynamics (matrices **A** and **B** are known). The use of the dynamic inversion principle increases the generality character of our new ALS; therefore, the designed system can be used both for the case when the aircraft dynamics are nonlinear and for the case when the aircraft dynamics are linear. Using the dynamic inversion, the command vector $±_c = [±_{p_c} \; ±_{T_c}]^T$ is obtained; by expressing from the state equation $\dot{\mathbf{x}} = \mathbf{Ax} + \mathbf{Bu} + \mathbf{B_v v_v}$, the first and the third differential equation, with **A**, **B**, and $\mathbf{B_v}$ having the above forms, the command vector components result as follows:

$$\begin{aligned} ±_{p_c} &= b_{31}^{¡1}(!_{y_c} ¡ a_{31} V_x ¡ a_{32} ® ¡ a_{33} !_y + a_{31} V_{vx} + a_{32}^{\cdot} V_{vz}) \\ ±_{T_c} &= b_{12}^{¡1}(\dot{V}_{x_c} ¡ a_{11} V_x ¡ a_{12} ® ¡ a_{14} \theta + a_{11} V_{vx} + a_{12}^{\cdot} V_{vz}): \end{aligned} \quad (7)$$

$!_{y_c}$ and V_{x_c} are the calculated values of the angular rate $!_y$ and the linear rate V_x, respectively. Equations (7) and the below equivalent form describe the inverse model of aircraft motion:

$$±_c = \begin{bmatrix} ±_{p_c} \\ ±_{T_c} \end{bmatrix} = [b_{31}^{¡1} \quad b_{12}^{¡1}] \left(\begin{bmatrix} !_{y_c} \\ \dot{V}_{x_c} \end{bmatrix} ¡ \begin{bmatrix} a_{31} & a_{32} & a_{33} & 0 \\ a_{11} & a_{12} & 0 & a_{14} \end{bmatrix} \mathbf{x} + \begin{bmatrix} a_{31} & a_{32}^{\cdot} \\ a_{11} & a_{12}^{\cdot} \end{bmatrix} \mathbf{v_v} \right). \quad (8)$$

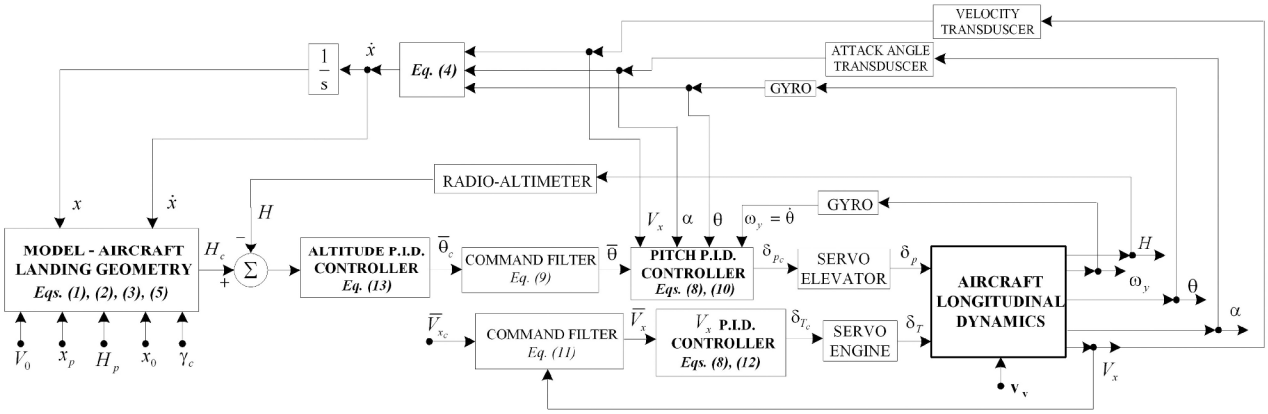

Fig. 2. New automatic control system for aircraft landing control.

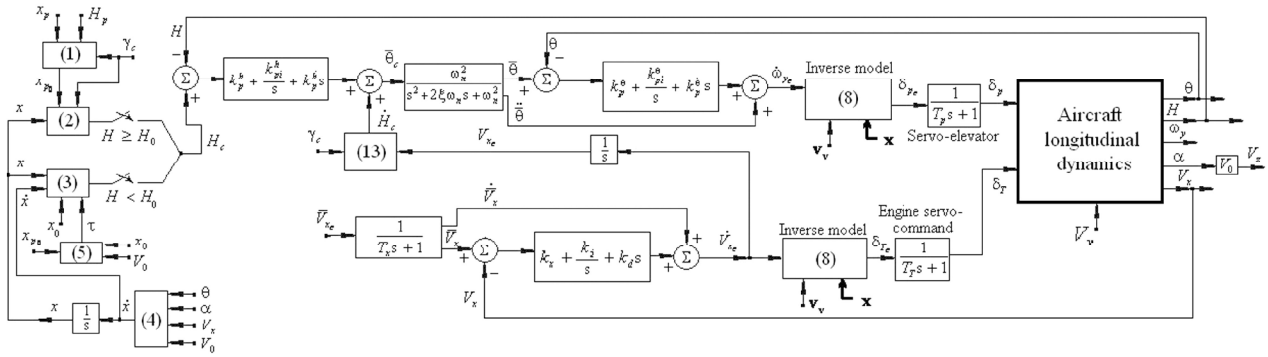

Fig. 3. Block diagram with transfer functions for system in Fig. 2.

According to [5] $\ddot{\gamma}_y$ is $\ddot{\gamma}_y = -\cos\psi\,\dot{\vartheta} + \dot{\psi}\cos\vartheta\sin\psi$ and, considering the assumption $\psi = \dot{\psi} = 0$ (ψ—roll angle and ψ—yaw angle), we obtain $\ddot{\gamma}_{y_c} = \ddot{\vartheta}_c$.

In order to obtain the command inputs of the flight control subsystems, we use command filters (reference filters) of order r. As a result, for the command of the pitch angle ϑ, we use the filter which is described by the equation:

$$\bar{\theta}(s) = \frac{\omega_n^2}{s^2 + 2\zeta\omega_n s + \omega_n^2}\bar{\theta}_c \tag{9}$$

with ω_n—natural pulsation, ζ—damping coefficient, and ϑ_c—calculated value of the pitch angle. With these we obtain the components of the angular rate control law [6]:

$$\ddot{\gamma}_{y_c} = \ddot{\vartheta}_c = \ddot{\bar{\theta}} + k_p^{\theta}(\dot{\bar{\theta}} - \dot{\theta}) + k_{pi}^{\theta}\int(\bar{\theta} - \vartheta)dt + k_p^{\theta}\frac{d}{dt}(\bar{\theta} - \theta): \tag{10}$$

For the command of speed V_x, a filter described by equation

$$\bar{V}_x = \bar{V}_{x_c}/(T_x s + 1) \tag{11}$$

is used; T_x is the filter time constant, while $\bar{V}_{x_c}$ is the desired value of the velocity V_x. The filter provides the signals $\bar{V}_x, \dot{\bar{V}}_x$ necessary for the calculation of the acceleration V_{x_c} [7]:

$$V_{x_c} = \ddot{\bar{V}}_x + k_x(\dot{\bar{V}}_x - V_x) + k_i\int(\bar{V}_x - V_x)dt + k_d\frac{d}{dt}(\dot{\bar{V}}_x - V_x): \tag{12}$$

The control laws of the subsystems for the pitch angle and V_x velocity control are described by (8), with $\ddot{\gamma}_{y_c}$ and V_{x_c} having the forms (10) and (12) (Fig. 2). We added to the four states a new state (the altitude H); its equation describes aircraft kinematics and may be written under the form $\dot{H} = V_0\dot{\gamma}$. For the altitude calculation a PID controller is used. This controller is described by (13) [11]:

$$\bar{\theta}_c = H_c + k_p^h(\dot{H}_c - \dot{H}) + k_i^h\int(H_c - H)dt + k_p^h\frac{d}{dt}(H_c - H) \tag{13}$$

where H_c is described by $\dot{H}_c = V_{x_c}\gamma_c$. The block diagram with transfer functions for the ALS is presented in Fig. 3. For better performances conventional controllers may be replaced by optimal, adaptive, or fuzzy controllers [12–14].

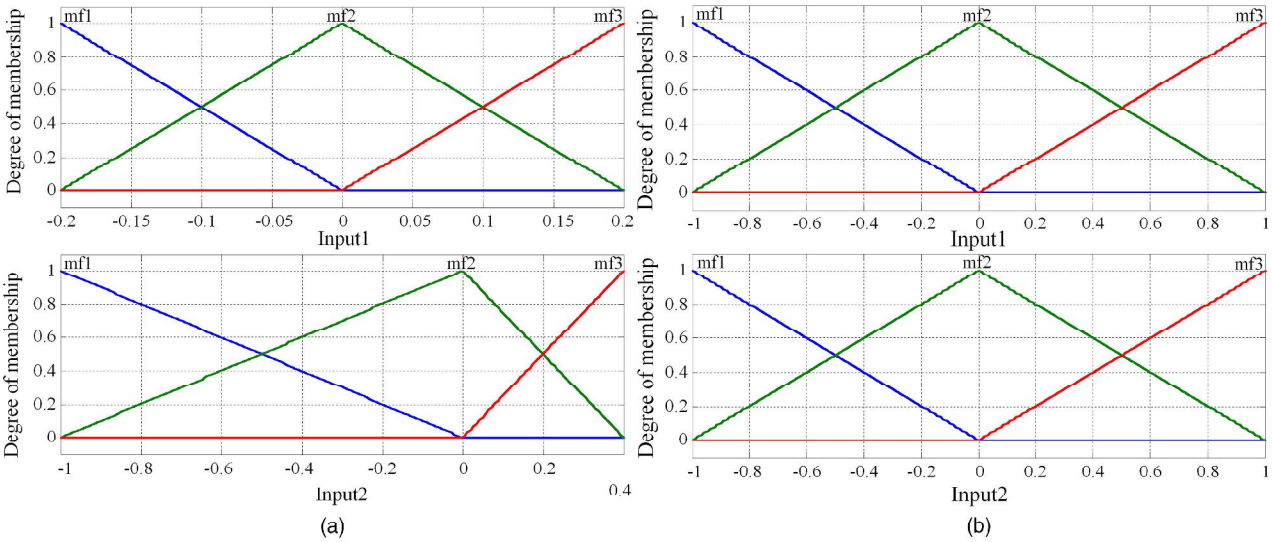

Fig. 4. Membership functions for inputs of fuzzy controllers.

V. THE DESIGN OF THE FUZZY LOGIC CONTROLLERS

Besides the conventional controllers we design fuzzy logic controllers (FLCs) to make our new ALS more robust and viable even in the case of complex nonlinear landing equations. Using multivalent fuzzy logic, linguistic expressions in antecedent and consequent parts of IF-THEN rules describing the operator's actions can be efficiently converted into control algorithms suitable for microcomputer implementation or implementation with specially designed fuzzy processors [10]. In contrast with traditional control theory, an FLC is not based on a mathematical model, and provides a certain level of artificial intelligence to conventional controllers; these methods are characterized by good adaptability and robustness.

In this section we develop three fuzzy controllers which may replace the conventional controllers. In our case the chosen fuzzy controllers are the "PID" type; this means that a PID dependence is realized between the input and the output [15]. Thus, three fuzzy controllers were developed for the control of altitude, pitch angle, and velocity. The second and the third controllers are identical from the fuzzy structure point of view, the differences appearing at the proportional, integral, and derivative coefficients obtained after the tuning process. The error and the change in error are the controllers' inputs, while the membership functions assigned for the inputs are of the triangular type. To reduce the computing time, we reduce the number of the membership functions and we simplify these functions. Membership functions (mf) for inputs are presented in Fig. 4. To define the rules a Sugeno fuzzy model was chosen (model proposed by Takagi, Sugeno, and Kang [16]). The next rules of the two fuzzy controllers have been chosen as

Rule 1: If e is A_1^1 and ¢e is A_2^1, then $y^1(e, ¢e) = ¡0{:}1$

Rule 2: If e is A_1^1 and ¢e is A_2^2, then $y^2(e, ¢e) = ¡0{:}05$

Rule 3: If e is A_1^2 and ¢e is A_2^1, then $y^3(e, ¢e) = ¡0{:}05$

Rule 4: If e is A_1^2 and ¢e is A_2^2, then $y^4(e, ¢e) = 0{:}005$

Rule 5: If e is A_1^2 and ¢e is A_2^3, then $y^5(e, ¢e) = 0{:}03$

Rule 6: If e is A_1^3 and ¢e is A_2^1, then $y^6(e, ¢e) = ¡0{:}1$

Rule 7: If e is A_1^3 and ¢e is A_2^2, then $y^7(e, ¢e) = 0{:}001$

Rule 8: If e is A_1^3 and ¢e is A_2^3, then $y^8(e, ¢e) = 0{:}005$: (14)

Rule 1: If e is A_1^1 and ¢e is A_2^1, then $y^1(e, ¢e) = ¡2$

Rule 2: If e is A_1^1 and ¢e is A_2^2, then $y^2(e, ¢e) = ¡1{:}6$

Rule 3: If e is A_1^1 and ¢e is A_2^3, then $y^3(e, ¢e) = 0$

Rule 4: If e is A_1^2 and ¢e is A_2^1, then $y^4(e, ¢e) = ¡1{:}6$

Rule 5: If e is A_1^2 and ¢e is A_2^2, then $y^5(e, ¢e) = 0$

Rule 6: If e is A_1^2 and ¢e is A_2^3, then $y^6(e, ¢e) = 1{:}6$

Rule 7: If e is A_1^3 and ¢e is A_2^1, then $y^7(e, ¢e) = 0$

Rule 8: If e is A_1^3 and ¢e is A_2^2, then $y^8(e, ¢e) = 1{:}6$

Rule 9: If e is A_1^3 and ¢e is A_2^3, then $y^9(e, ¢e) = 2$: (15)

A_q^i ($q = \overline{1,2}$, $i = \overline{1,3}$) are the individual antecedent fuzzy sets of each input variable, e—the error and ¢e—the change in error.

VI. NUMERICAL SIMULATION RESULTS

To study the performances of the new ALS, we consider a Charlie-1 aircraft with the following stability derivates [1]:

$$X_u = -0.021[1/s], \quad X_w = 0.122[1/s]$$

$$Z_u = -0.2[1/s], \quad Z_w = -0.512[1/s]$$

$$V_0 \cong V_{x_0} = 67[m/s], \quad N_w = -0.006[deg/(s\cdot m)]$$

$$N_{\dot{w}} = -8\cdot 10^{-4}[deg/m], \quad X_{\delta_T} = 3.66\cdot 10^{-6}[(m/s)/deg]$$

$$Z_{\delta_T} = -1.69\cdot 10^{-7}[(m/s)/deg], \quad N_{\delta_T} \cong 0$$

$$Z_{\delta_p} = -1.96[(m/s)/deg], \quad N_{\delta_p} = 0$$

$$\sin\theta_0 \cong 0, \quad \cos\theta_0 \cong 1, \quad Z_u^{\cdot} = Z_u/V_0:$$

The coordinates of point A_p have been chosen as $H_p = 100$ m, $x_p = 0$ m. The trajectory slope is $\theta_c = -2.5$ deg, while the other parameters in Fig. 3 have these values: $T_x = 5$ s, $T_p = 0.01$ s, $T_T = 5$ s, $\omega_n = 3$ rad/s, $\xi = 0.7$, $\xi = 0.7$, $\bar{V}_{x_c} = 67$ m/s. The following values of the controller parameters have been obtained using the well-known Ziegler-Nichols tuning method:

$$k_p = 50[(deg/s^2)/deg], \quad k_{pi}^{\theta} = 10[(deg/s^3)/deg]$$

$$k_p^{\theta} = 2[(deg/s^2)/(deg/s)], \quad k_p^h = 0.5[deg/m]$$

$$k_{pi}^h = 10^{-4}[(deg/s)/m], \quad k_p^{\dot{h}} = 0.5[deg/(m/s)]$$

$$k_x = 20[(m/s^2)/(m/s)], \quad k_i = 0.01[(m/s^3)/(m/s)]$$

$$k_d = 14.$$

A. Validation of the ALS with Conventional Controllers

In Fig. 5 and Fig. 6 we represent the time characteristics for the glide slope landing phase and flare landing phase, respectively in the presence or in the absence of the wind shears which are modeled by (6) with $T_0 = 60$ s, $V_{vx_0} = 10$ m/s, $V_{vz_0} = 15$ m/s. To be sure that the new ALS responds well to wind shears, we have chosen values of V_{vx_0} and V_{vz_0} bigger than their medium values.

The presence of the wind shears is not very visible. The curves with solid line (without wind shears) overlap almost perfectly over the curves plotted with dashed line (with wind shears). The time origin for the flare trajectory is chosen as zero when the altitude is $H = H_0 = 20$ m (the altitude at which the glide slope ends).

In the above simulations we did not take into consideration the errors of the sensors (the sensors are used for the measurement of the states). The errors of the gyro sensors in the pitch channel are considered in simulations below. For the determination of the pitch angle we may use an integrator gyro. This gyro has errors and it is interesting to see if the sensor errors affect the landing; its error model takes into account the parameters from data sheets offered by the sensor producers. The error model is described by the equation:

$$\theta = (\theta_i + S\cdot a_r + B + \nu)(1 + \Delta K/K): \tag{16}$$

θ is the output pitch angle (the perturbed signal), θ_i—input pitch angle, S—sensibility to the acceleration a_r applied on an arbitrary direction, B—bias, K—scale factor, ΔK—calibration error of the scale factor, and ν—sensor noise. This error model has been introduced in the ALS model in the feedback after the pitch angle θ. In the error model the bias is given by its maximum value B as the percentage of span; the calibration error of the scale factor is given by its absolute maximum value ΔK as the percentage of K; the noise is given by using its maximum density value. The inputs of the error model are: pitch angle θ_i and acceleration a_r, considered to be the resultant acceleration signal that acts upon the carrier vehicle, while the output is the disturbed pitch angle θ. In the numerical simulation the following parameters have been used: noise density: $5.8\cdot 10^{-6}$[deg=$\sqrt{Hz}$], bias: $9.8\cdot 10^{-8}$[deg], error of the scale factor: $5.2\cdot 10^{-4}\%\cdot K$, sensibility to accelerations $\cong 0$[deg=g]; g—gravitational acceleration. Figures 7 and 8 depict the time characteristics of the ALS, with conventional controllers, taking into account the absence or presence of gyro sensor errors. Although these errors affect some variables, time variation of altitude and landing phases time length are not affected. So, sensor errors do not affect landing.

In Table I we present, for the most important 5 variables, the influences of the wind shears and errors of the sensor upon the parameters maximum absolute deviation with respect to their steady values. From the values in Table I it can be noticed that the sensor errors have less significant influence on the steady-state values of the variables; generally, the ratio of the errors induced by the turbulences and sensor errors is 3 : 1.

REMARK 1 From the theoretical part of this paper, we retain the mandatory values of the slope angle: -2.5 deg (first landing phase) and 0 deg (second landing phase). Analyzing Figs. 5–8 we remark on the correctness of the simulation data; thus, for the glide slope (Figs. 5 and 7) the aircraft slope angle tends to be the desired value in about 7 s, while, for the flare phase (Figs. 6 and 8) it tends to be the desired value in about 9 s. In the glide slope phase, the aircraft must have a linear descendent trajectory (last graphic of Fig. 5) and, therefore, the pitch angle must be negative; as one can see in Figs. 5 and 7, the pitch angle is -2.3 deg, while the attack angle is slightly positive ($\cong 0.2$ deg); it results in the desired slope angle (-2.5 deg). In the flare phase aircraft must describe a parabolic trajectory (last graphic of Fig. 6)

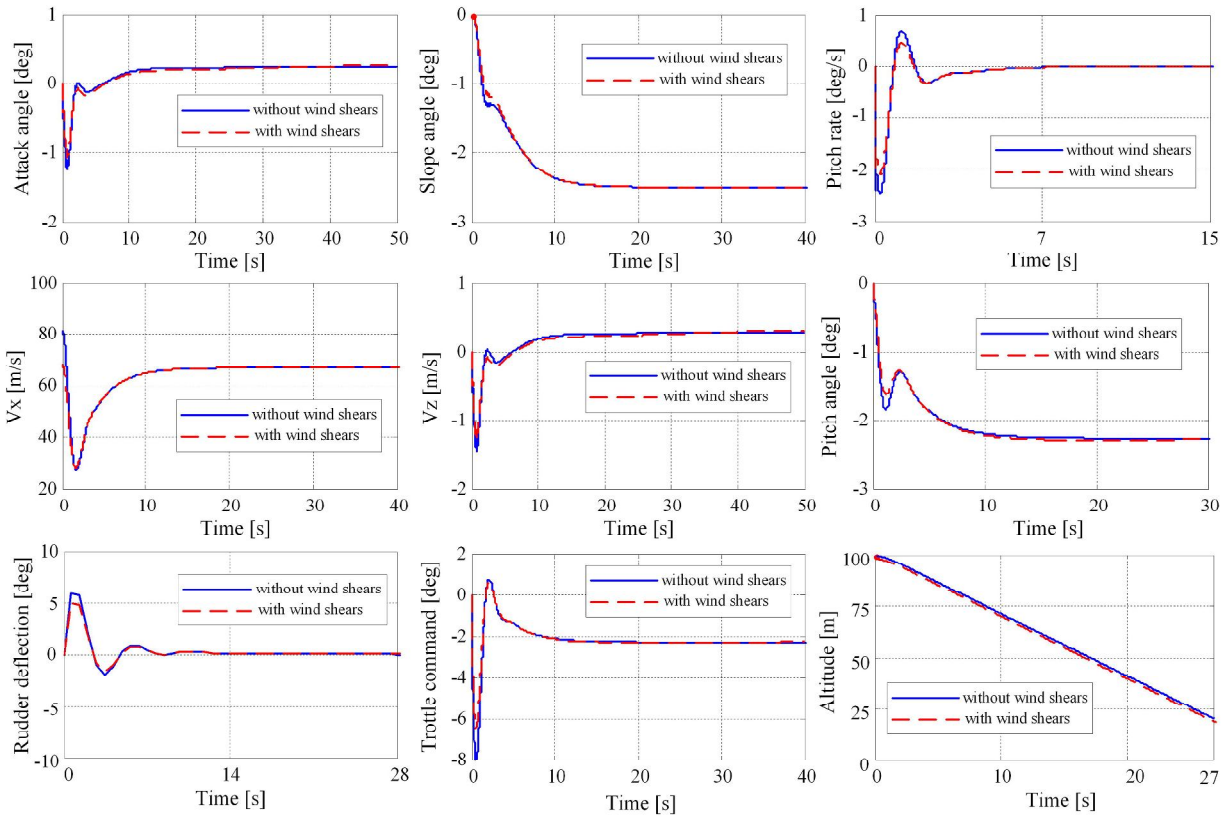

Fig. 5. Time characteristics of ALS with PID controllers, for glide slope phase, with or without wind shears.

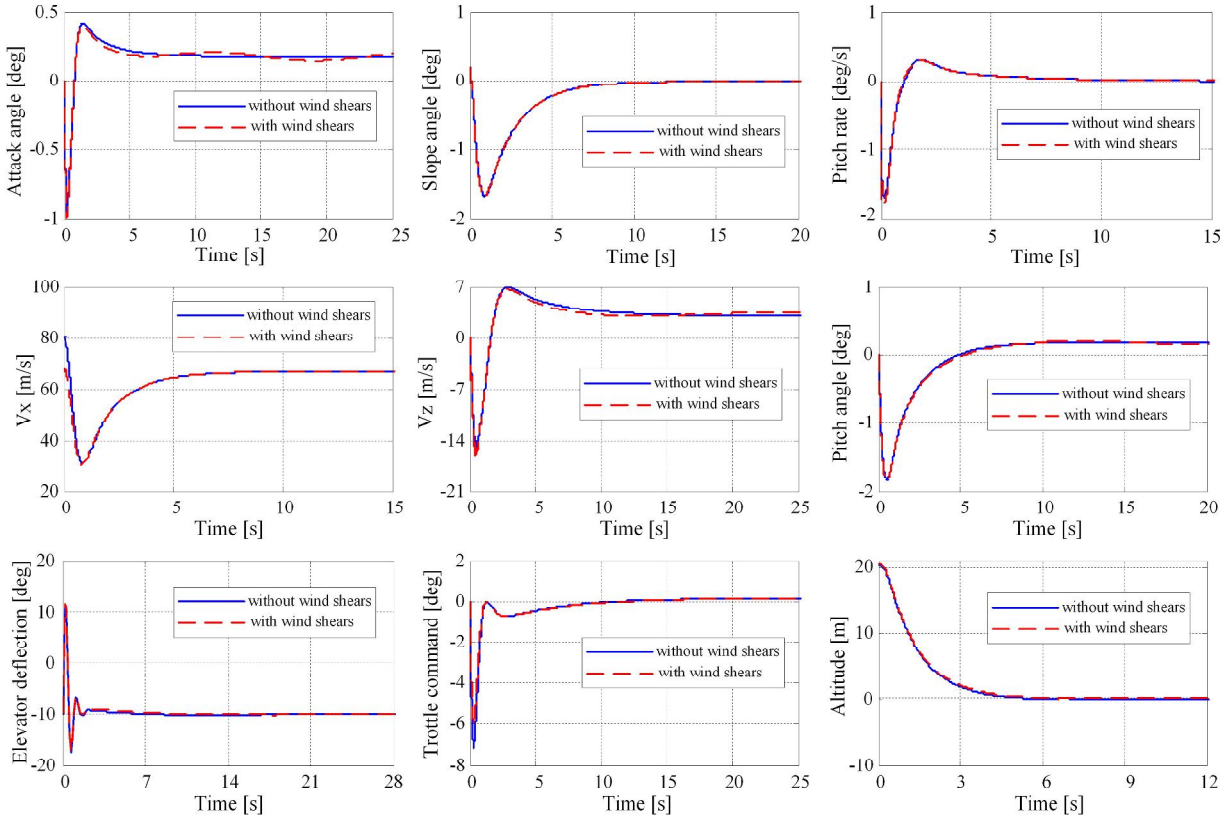

Fig. 6. Time characteristics of ALS with PID controllers, for flare phase, with or without wind shears.

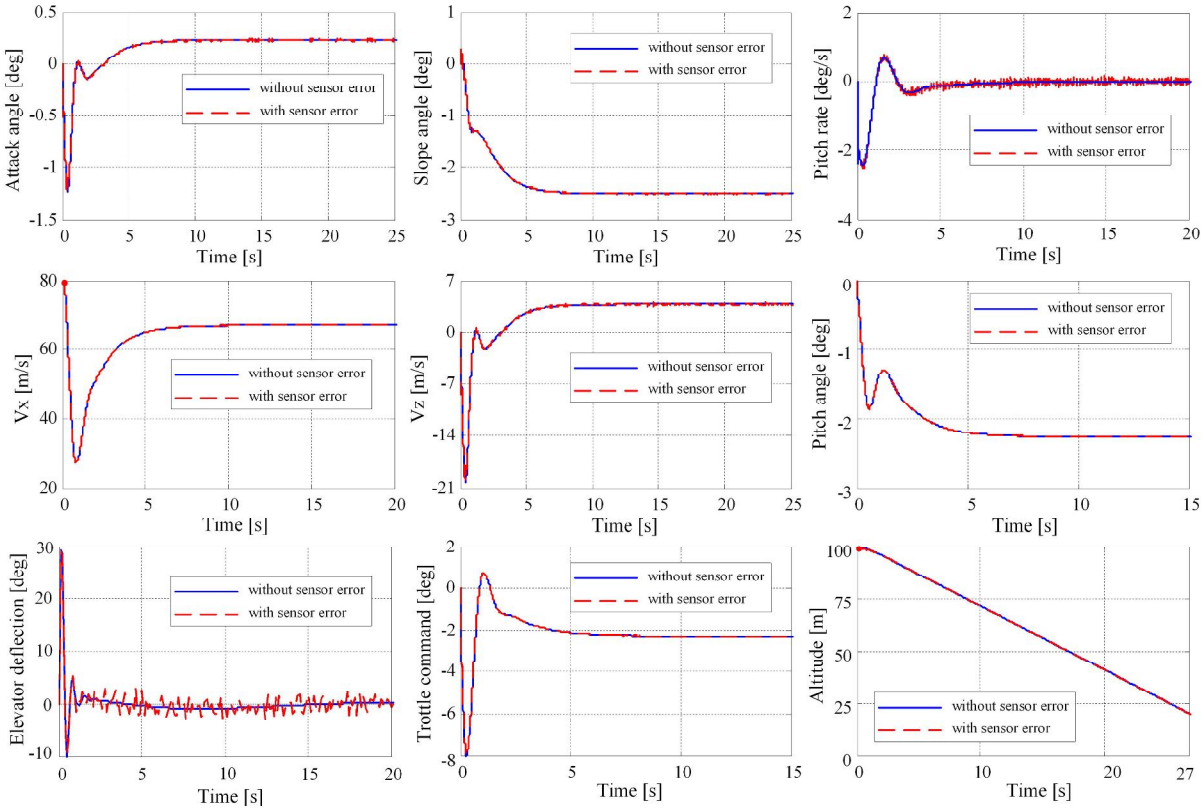

Fig. 7. Time characteristics of ALS with PID controllers, for glide slope phase, taking into account absence or presence of sensor errors.

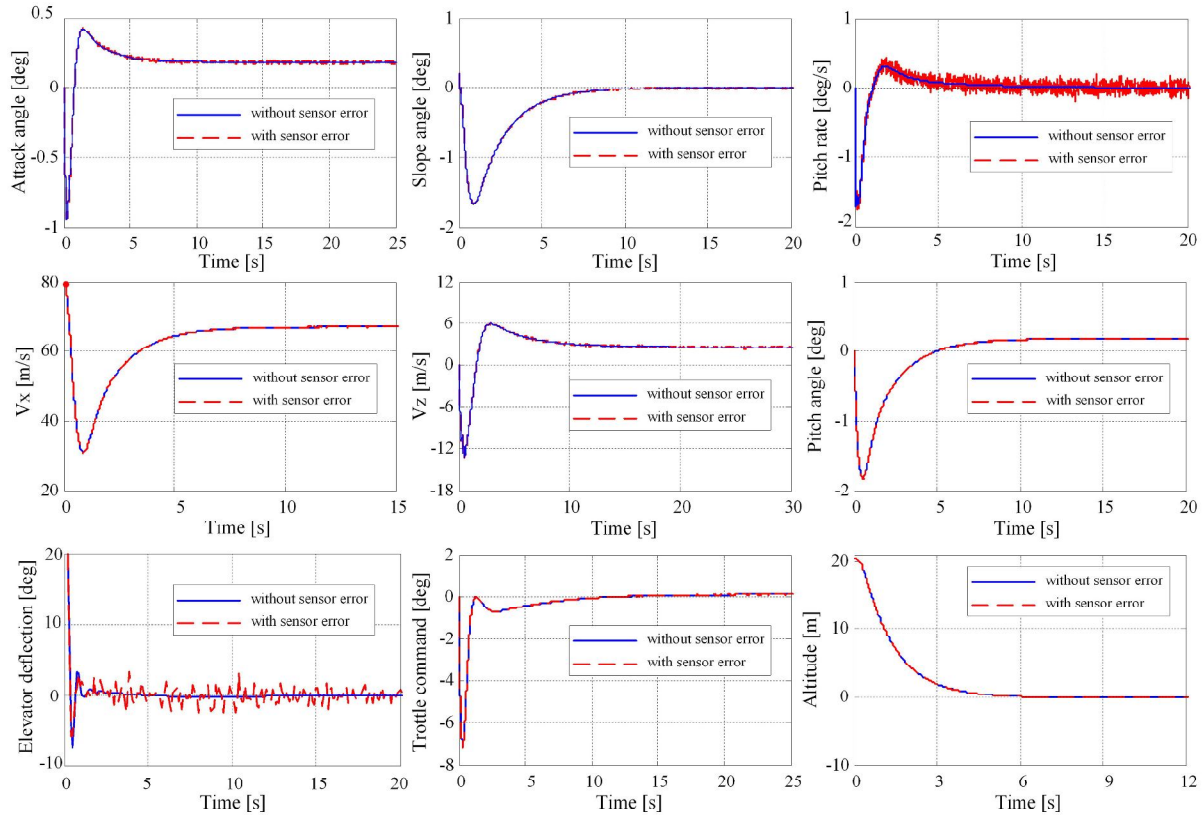

Fig. 8. Time characteristics of ALS with PID controllers, for flare phase, taking into account absence or presence of sensor errors.

with a null slope angle; in Figs. 6 and 8, the pitch angle is slightly positive (0.2 deg), while the attack angle is slightly positive too (0.2 deg); it results in the desired null slope angle. On the other hand the pitch angle is controlled by means of the elevator; after the pitch angle stabilization (about 7 s), the elevator must not be deflected any more and, as a consequence, after 7 s, the elevator deflection remains at its steady null value (Figs. 5–8)).

B. Comparison between the Two Variants of ALS

Replacing the conventional controllers with fuzzy controllers in the ALS structure, dynamic characteristics with superior quality indicators are obtained; moreover, the fuzzy controllers have the advantage of very good adaptability, robustness, and software implementation capabilities.

Figures 9 and 10 expose the time characteristics of the ALS, with conventional controllers (solid line) and fuzzy controllers (dashed line), while in Fig. 11 the characteristics H(x), for the 2 cases (conventional and fuzzy controllers), are represented.)

REMARK 2 The aim of the controllers' design, by using the fuzzy control technique, was to improve the system performances (damping, overshoot (OVS), and transient regime period (TRP)). From the damping point of view, we see a decrease especially in the case of pitch angular rate and elevator deflection for ALS with fuzzy controllers with respect to the ALS with conventional controllers.

In Table II a comparison for the most important 5 variables, between the OVS and the TRP for the two variants of ALS is achieved; it can be concluded that the fuzzy control improves significantly the variables' OVS. From the TRP point of view, the values are approximately the same, with a slight advantage for the ALS with fuzzy controllers. For OVS the conventional/fuzzy variants improvement ratios are: 2.45 times (phase 1) and 1.57 times (phase 2)—attack angle; 1.32 times (phase 2)—pitch angle (phase 1: damped response for fuzzy controllers); 1.27 times (phase 2)—slope angle (phase 1: damped responses for both controls); 1.23 times (phase 1) and 1.13 times (phase 2)—V_x velocity; 2.19 times (phase 1), 1.7 times (phase 2)—V_z velocity.

For Charlie-1 aircraft, the glide slope phase takes approximately 26.9 s, while the flare phase takes approximately 6.1 s; the steady values of longitudinal and vertical velocity are $V_x \cong 67$ m/s and $V_z \cong 3$ m/s, respectively. By using this information, one makes a brief analysis regarding the numerical simulation data correctness: 1) horizontal distance covered by aircraft in the first landing phase must be approximately 67 m/s¢26:9s = 1802:3 m, while, in the second landing phase, it must be approximately 67 m/s¢6:1s = 408:7 m (Fig. 11); 2) vertical distance covered by aircraft must be 3 m/s¢26:9s = 80:7 m (phase 1) and 3 m/s¢6:1s = 18:3 m (phase 2). These values are again confirmed by Fig. 11: phase 1 means an 80 m descent for aircraft center of gravity, while phase 2 means a 20 m descent; the difference of 1.7 m appears because the aircraft center of gravity is approximately 1.7 m above the ground.

REMARK 3 We can see that some of the variables have big amplitudes at the landing beginning; because we do not have any information regarding the trim conditions which lead to the stability derivates, our initial conditions (V_x = 80 m/s, ® = = 0 deg, $!_y$ = 0 deg/s) were easily different from these trim condition.

C. Validation of the ALS with Fuzzy Controllers

Figures 12 and 13 depict the time characteristics of the ALS, with PID fuzzy controllers, taking or not taking into consideration the wind shears. Wind shears affect the transient regime of the two phases in an insignificant manner: steady regime is not affected, while TRP is approximately the same for the two cases.

Figures 14 and 15 depict the time characteristics of the ALS with PID fuzzy controllers. The sensor errors produce an increase of the signals amplitude in the transient regime and very small oscillations in the steady regime, but these errors do not affect the two landing phases. Wind shears and sensor errors influences upon the parameters' maximum absolute deviation with respect to their steady values are presented in Table III. An errors' level reduction can be seen if fuzzy controllers are used.

REMARK 4 The biggest absolute deviations with respect to the steady values appear for vertical velocity V_z (about 11–13 times bigger for ALS with conventional controllers—Table I and about 10–12 times bigger for the ALS with fuzzy controllers—Table III); therefore, the wind shears and sensor errors affect in principal the vertical velocity and affect less the attack and pitch angles, and so on. Usually, an influence on the vertical speed is equivalent, from the landing point of view, with an influence on the flight altitude. These deviations can be considered as additional disturbance acting upon aircraft during landing. In phase 1 this disturbance (vertical wind shear) has no effect (Fig. 11)—aircraft trajectory is linear (both variants of ALS); a difference appears in phase 2 when wind shears can be more dangerous. Here, the vertical velocity increase for ALS with conventional controllers (Fig. 11) leads to faster ground approach (1 s); although the aircraft reaches the ground with 1 s delay, the flare for the ALS with fuzzy controllers is smoother. The little hump (ALS with conventional controller) is a disadvantage.

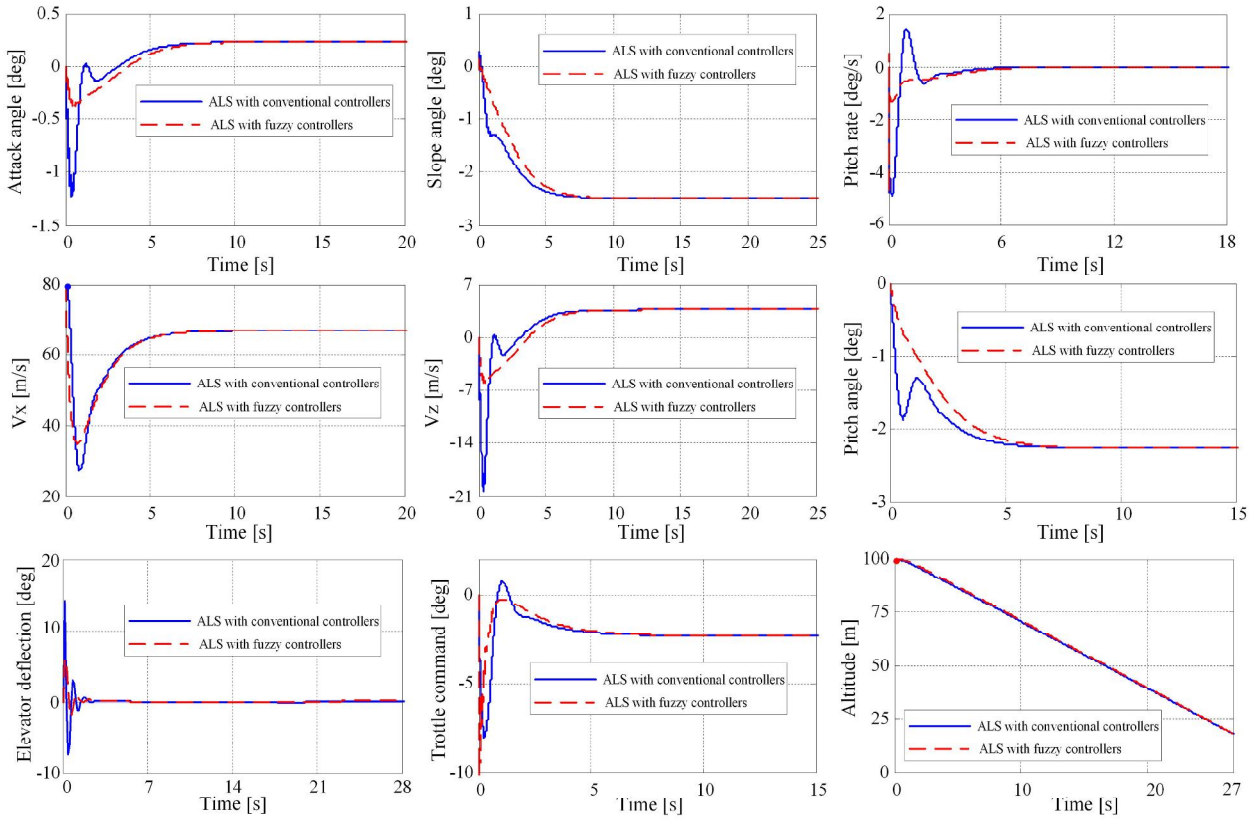

Fig. 9. Time characteristics of ALS with PID conventional and fuzzy controllers for glide slope phase.

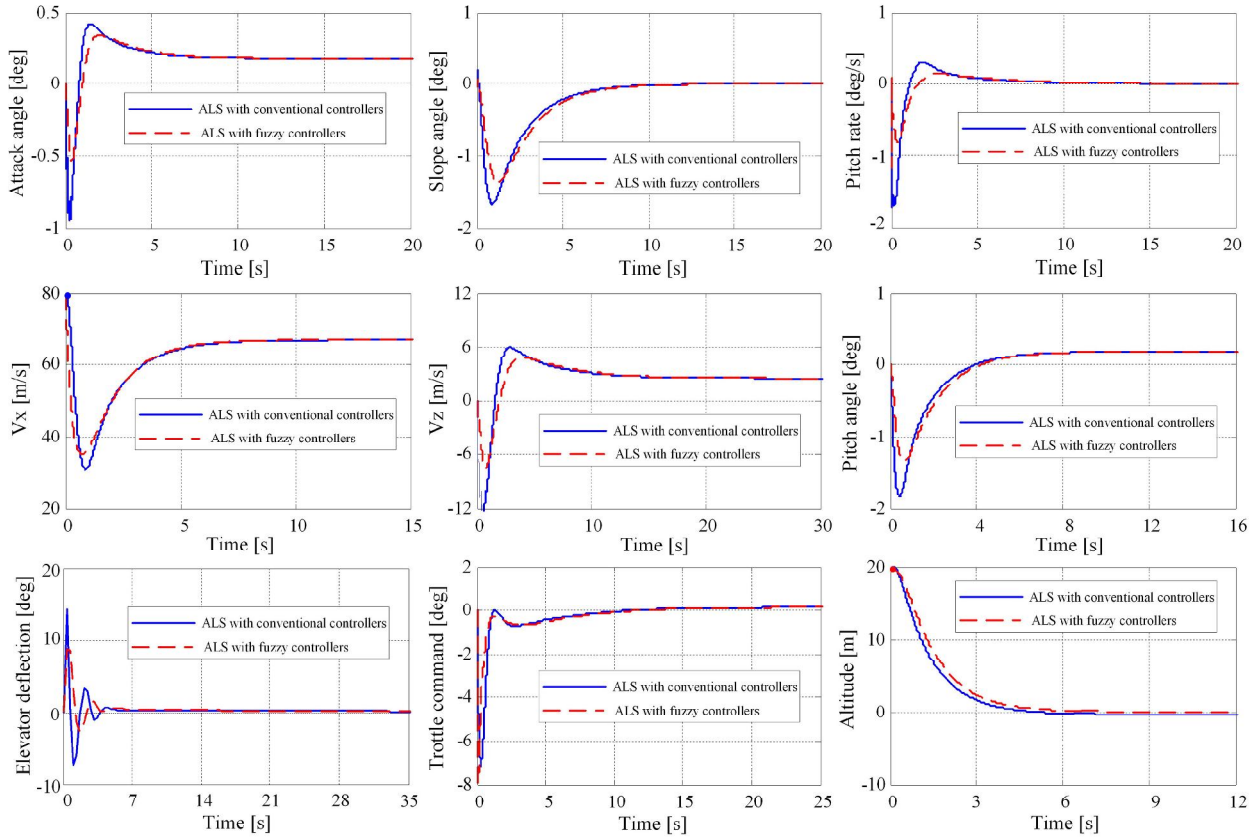

Fig. 10. Time characteristics of ALS with PID conventional and fuzzy controllers for flare phase.

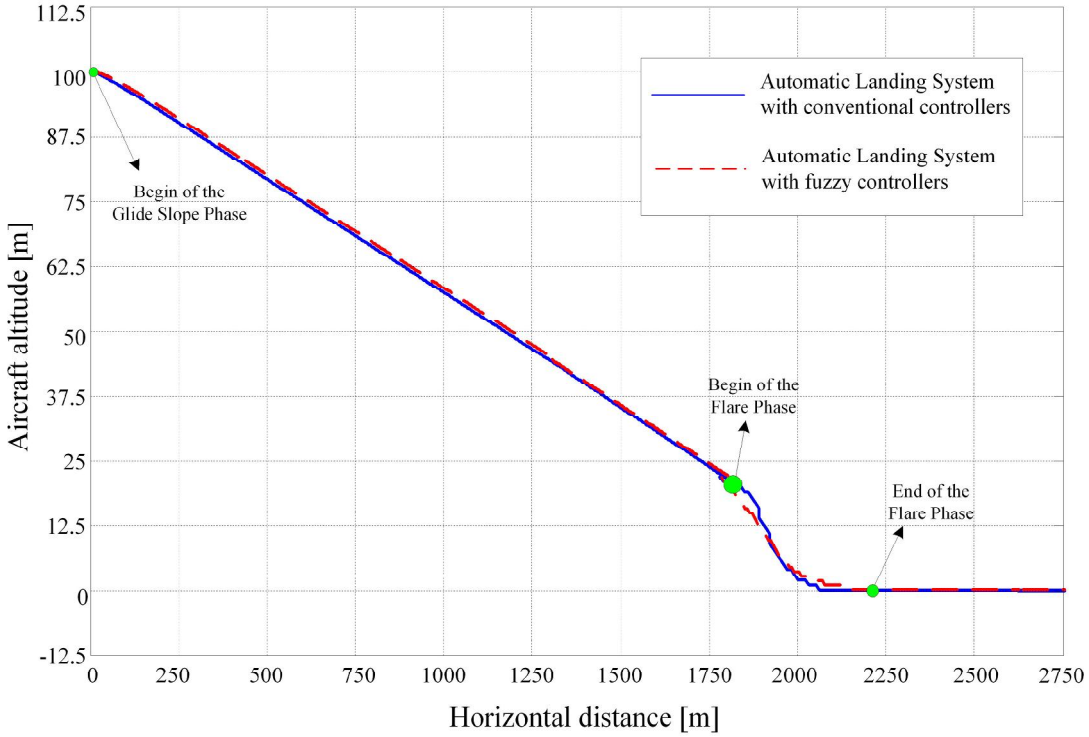

Fig. 11. Characteristics H(x) for ALS with conventional/fuzzy controllers.

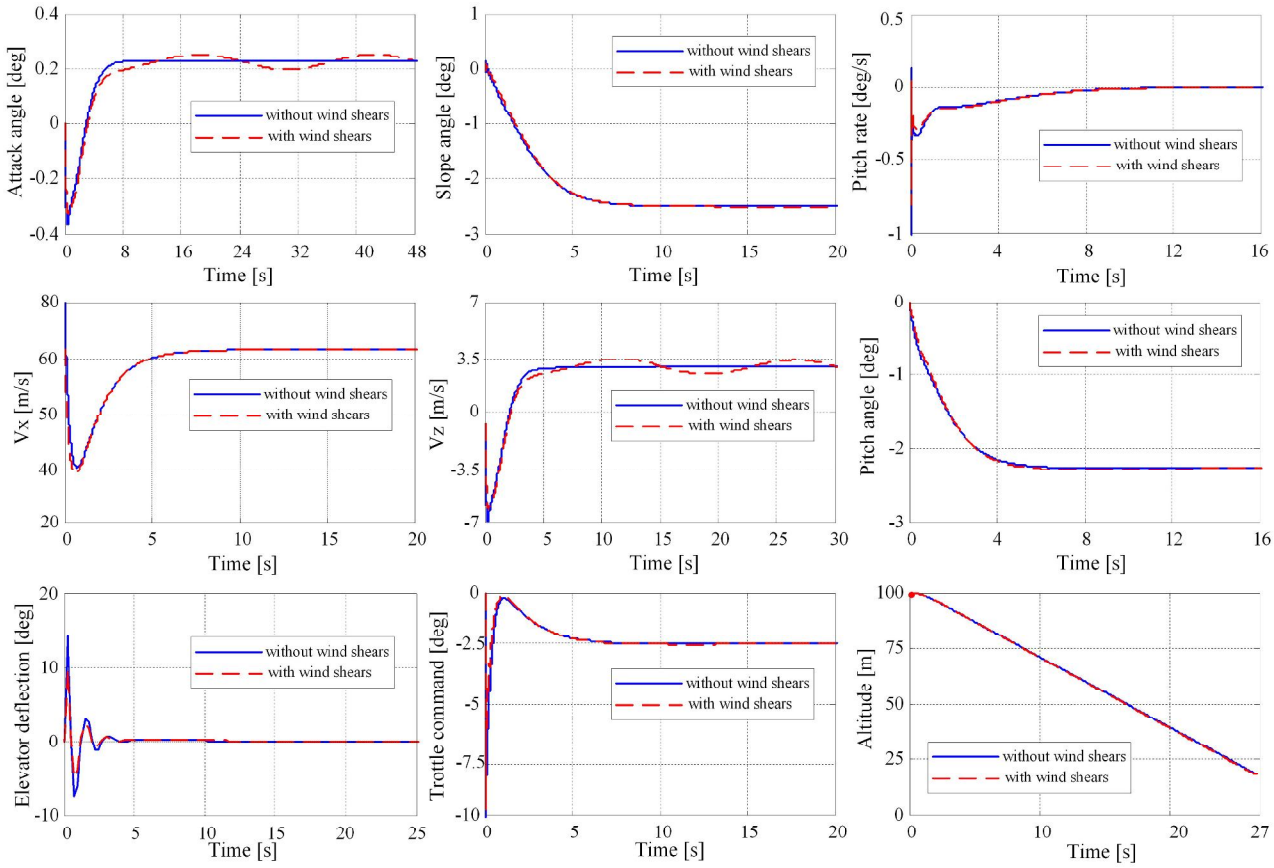

Fig. 12. Time characteristics of ALS with fuzzy controllers, for glide slope phase, with or without wind shears.

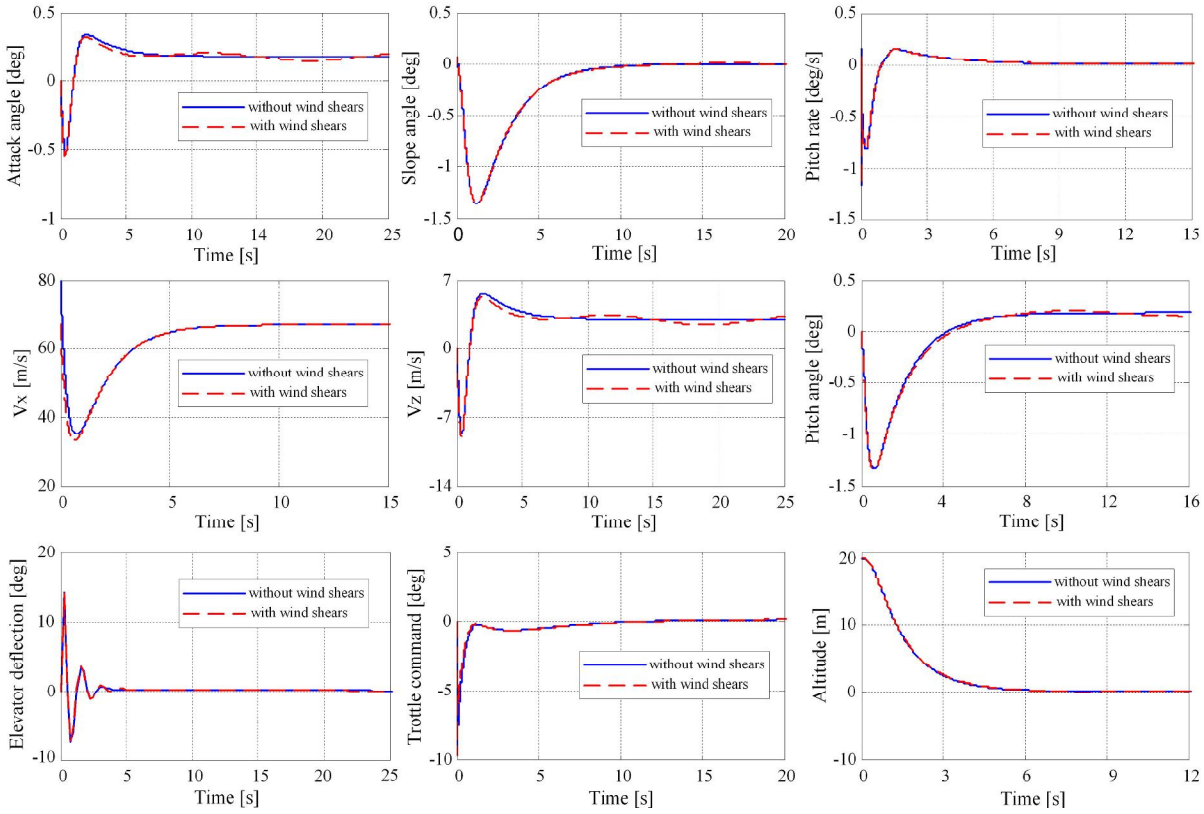

Fig. 13. Time characteristics of ALS with fuzzy controllers, for flare phase, with or without wind shears.

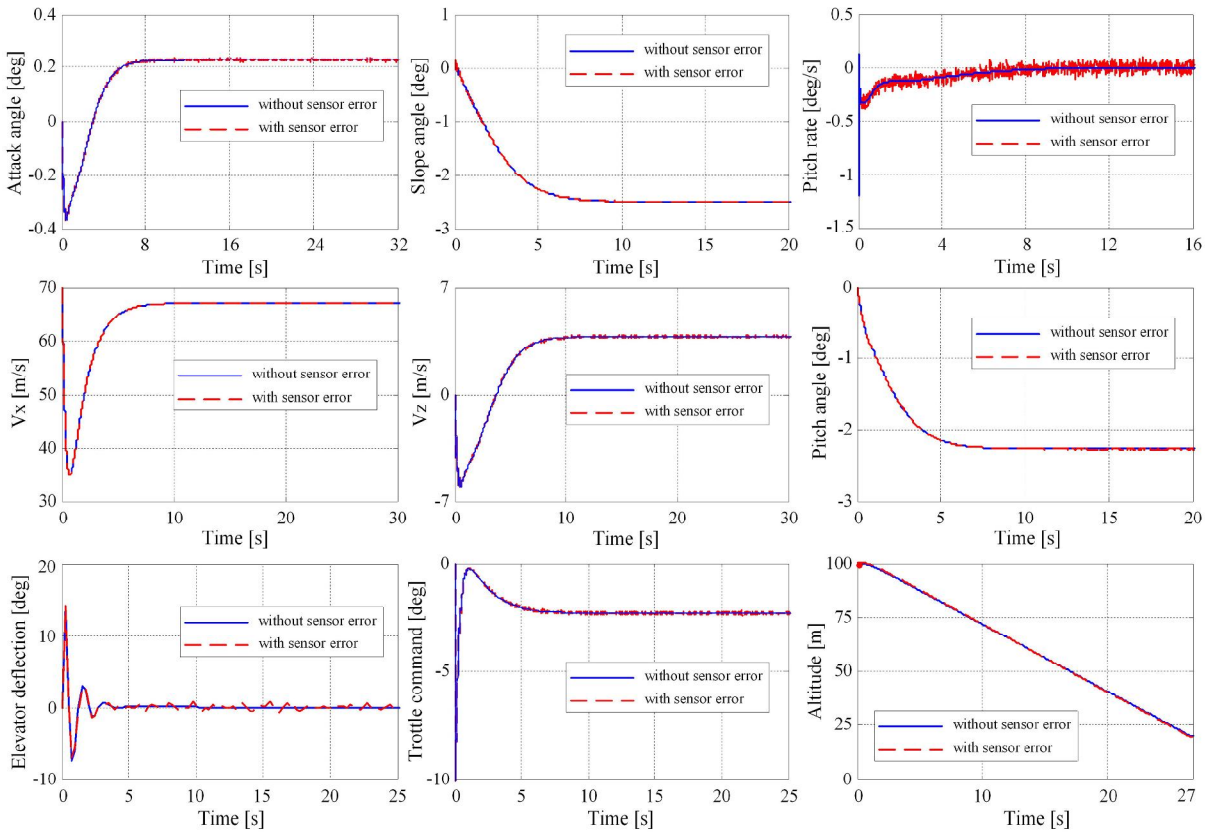

Fig. 14. Time characteristics of ALS with fuzzy controllers, for glide slope phase, considering or not considering sensor errors.

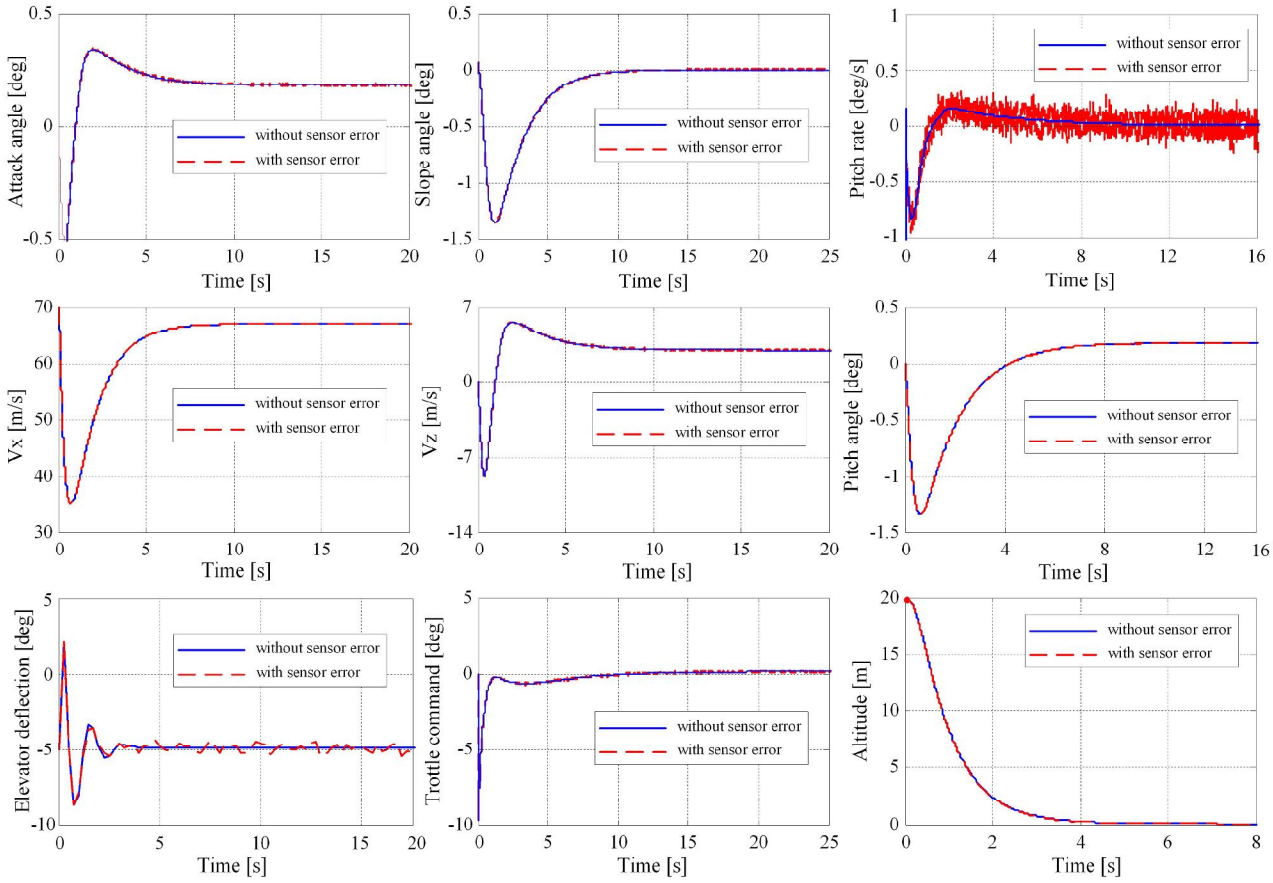

Fig. 15. Time characteristics of ALS with fuzzy controllers, for flare phase, considering or not considering sensor errors.

TABLE I
Parameters Maximum Absolute Deviation with Respect to their Steady Values (ALS with PID Controllers)

Parameters' Maximum Absolute Deviation	® [deg]		θ [deg]		° [deg]		V_x [m/s]		V_z [m/s]	
	Phase 1	Phase 2	Phase 1	Phase 2	Phase 1	Phase 2	Phase 1	Phase 2	Phase 1	Phase 2
ALS with wind shears	0.0235	0.0314	0.031	0.0298	0.0045	0.00469	0.0162	0.0228	0.4416	0.4356
ALS with sensor errors	0.0124	0.0141	0.0041	0.0061	0.0136	0.0119	0.0722	0.077	0.1764	0.2388

TABLE II
Quality Indicators for ALS with Conventional Controllers and ALS with Fuzzy Controllers

Variable		Attack Angle		Pitch Angle		Slope Angle		Velocity V_x		Velocity V_z	
Quality Indicators		OVS [deg]	TRP [s]	OVS [deg]	TRP [s]	OVS [deg]	TRP [s]	OVS [deg]	TRP [s]	OVS [deg]	TRP [s]
ALS (PID)	Glide slope phase	1.4635	7	0.95	7	0	7	39.65	7	20.548	7
	Flare phase	1.126	9	2.012	9	1.68	9	36.12	8	18.792	10
ALS (fuzzy)	Glide slope phase	0.5982	6.6	0	6.6	0	6.6	32.1	7	9.394	6.5
	Flare phase	0.716	8.5	1.52	8.5	1.326	8.5	32.02	8	11.02	10

VII. CONCLUSION

Simulation results show that the new ALS has been shown to perform well in its ability to track the desired flight path angle during glide slope and flare. Wind shears have the biggest influence on the system variables, while sensor errors have the lowest one. For the designed ALS, the following original issues can be mentioned: 1) the landing geometry; 2) the design of the PID controller for the altitude H, design of the command filter and PID controller for pitch angle, synthesis of the control law $\pm_{p_c}$ using the

TABLE III
Parameters Maximum Absolute Deviation with Respect to their Steady Values (ALS with Fuzzy Controllers)

Parameters' Maximum Absolute Deviation	® [deg]		θ [deg]		° [deg]		V_x [m/s]		V_z [m/s]	
	Phase 1	Phase 2	Phase 1	Phase 2	Phase 1	Phase 2	Phase 1	Phase 2	Phase 1	Phase 2
ALS with wind shears	0.0242	0.032	0.0225	0.0297	0.0074	0.0073	0.0002	0.0002	0.3432	0.4488
ALS with sensor errors	0.0075	0.0069	0.0035	0.0035	0.0089	0.0086	0.0036	0.0032	0.1128	0.114

dynamic inversion; 3) the design of the PID controller for velocity V_x, synthesis of the control law $\pm_{T_c}$, and the afferent command filter design; 4) the control laws of the three controllers (conventional or fuzzy) are chosen such that the system is easily configurable: the signals provided by the transducers for the velocity V_x and pitch angle may be replaced by a strap-down inertial navigator; velocity V_x is obtained by the integration with respect to time of the signal provided by an accelerometer a_x (placed along aircraft longitudinal axis), while the pitch angle is obtained by the integration with respect to time of the signal provided by the pitch angular rate gyro ($!_y$); this signal, together with the one provided by an attack angle sensor, are used to calculate the flight path angle °, descent velocity H, and altitude H (without using an altimeter); so, only three sensors are necessary: a sensor for a_x, a sensor for ®, and a sensor for $!_y$; 5) the study of the errors induced by wind shears and gyro errors, using conventional and fuzzy controllers.

ROMULUS LUNGU
MIHAI LUNGU
LUCIAN TEODOR GRIGORIE
University of Craiova
Faculty of Electrical Engineering
107 Decebal Street
200440 Craiova
Romania
E-mail: (Lma1312@yahoo.com)

REFERENCES

[1] McLean, D.
Automatic Flight Control Systems.
Upper Saddle River, NJ: Prentice-Hall, 1990.

[2] Singh, S. and Padhi R.
Automatic landing of unmanned aerial vehicles using dynamic inversion.
Proceedings of the International Conference on Aerospace Science and Technology, Bangalore, India, June 26–28, 2008.

[3] Juang, J. G. and Cheng, K. C.
Application of neural network to disturbances encountered landing control.
IEEE Transactions on Intelligent Transportation Systems, **7**, 4 (2006), 582–588.

[4] Che, J. and Chen, D.
Automatic landing control using H-inf control and stable inversion.
Proceedings of the 40th Conference on Decision and Control, Orlando, FL, 2001, pp. 241–246.

[5] Lungu, M.
Sisteme de Conducere a Zborului.
Effretikon, Switzerland: Sitech Publisher, 2008.

[6] Kawaguchi, J. I., Miyazawa, Y., and Ninomiya, T.
Flight control law design with hierarchy—Structured dynamic inversion approach.
Presented at the AIAA Guidance, Navigation and Control Conference Exhibit, Honolulu, HI, 2008.

[7] Pashilkar, A. A., Sundararajan, N., and Saratchhandran, P. A.
Fault-tolerant neural aided controller for aircraft auto-landing.
Aerospace Science and Technology, **10**, 1 (2006), 49–61.

[8] Rong, H-J., et al.
Adaptive fuzzy fault-tolerant controller for aircraft autolanding under failure.
IEEE Transactions on Aerospace and Electronic Systems, **43**, 4 (2007), 1586–1603.

[9] Wang, J. and Gao, Y.
Land vehicle dynamics-aided inertial navigation.
IEEE Transactions on Aerospace and Electronic Systems, **46**, 4 (2010), 1638–1653.

[10] Kovacic, Z. and Bogdan, S.
Fuzzy Controller Design—Theory and Applications.
New York: Taylor and Francis, 2006.

[11] Tudosie, A.
Jet engine's speed controller with constant pressure chamber.
Proceedings of the International Conference on Automation and Information (ICAI'08), Bucharest, Romania, June 26–28, 2008, pp. 229–234.

[12] Doyle, J., et al.
Mixed H_2=H_1 performance objectives: Optimal control.
IEEE Transactions on Automatic Control, **39**, 8 (1994), 1575–1587.

[13] Kargin, V.
Design of an autonomous landing control algorithm for a fixed wing UAV.
M.S. thesis, Ankara University, Turkey, 2007.

[14] Mori, R. and Suzuki, S.
Neural network modeling of lateral pilot landing control.
Journal of Aircraft, **46** (2009), 1721–1726.

[15] Kumar, V., Rana, K., and Gupta, V.
Real-time performance evaluation of a fuzzy PI+fuzzy PD controller for liquid-level process.
International Journal of Intelligent Control and Systems, **13**, 2 (2008), 89–96.

[16] Mahfouf, M., Linkens, D., and Kandiah, S.
Fuzzy Takagi-Sugeno Kang Model Predictive Control for Process Engineering.
London: IEE Savoy Place Publisher, 1999.